Structural Model of the Human BTG2–PABPC1 Complex by Combining Mutagenesis, NMR Chemical Shift Perturbation Data and Molecular Docking

Aalam Ameerul [1], **Hibah Almasmoum** [1,2], **Lorenzo Pavanello** [1†], **Cyril Dominguez** [3] and **Gerlof Sebastiaan Winkler** [1*]

1 - *School of Pharmacy,* University of Nottingham, East Drive, University Park, Nottingham NG7 2RD, UK

2 - *Department of Laboratory Medicine,* Faculty of Applied Medical Sciences, Umm Al-Qura University, Makkah, Saudi Arabia

3 - *Leicester Institute of Structural & Chemical Biology and Department of Molecular & Cell Biology,* University of Leicester, Leicester LE1 7RH, UK

Correspondence to Gerlof Sebastiaan Winkler: sebastiaan.winkler@nottingham.ac.uk (G.S. Winkler)
https://doi.org/10.1016/j.jmb.2022.167662
Edited by David Mathews

Abstract

Degradation of cytoplasmic mRNA in eukaryotes involves the shortening and removal of the mRNA poly (A) tail by poly(A)-selective ribonuclease (deadenylase) enzymes. In human cells, BTG2 can stimulate deadenylation of poly(A) bound by cytoplasmic poly(A)-binding protein PABPC1. This involves the concurrent binding by BTG2 of PABPC1 and the Caf1/CNOT7 nuclease subunit of the Ccr4-Not deadenylase complex. To understand in molecular detail how PABPC1 and BTG2 interact, we set out to identify amino acid residues of PABPC1 and BTG2 contributing to the interaction. To this end, we first used algorithms to predict PABPC1 interaction surfaces. Comparison of the predicted interaction surface with known residues involved in the binding to poly(A) resulted in the identification of a putative interaction surface for BTG2. Subsequently, we used pulldown assays to confirm the requirement of PABPC1 residues for the interaction with BTG2. Analysis of RNA-binding by PABPC1 variants indicated that PABPC1 residues required for interaction with BTG2 do not interfere with poly(A) binding. After further defining residues of BTG2 that are required for the interaction with PABPC1, we used information from published NMR chemical shift perturbation experiments to guide docking and generate a structural model of the BTG2-PABPC1 complex. A quaternary poly(A)-PABPC1-BTG2-Caf1/CNOT7 model showed that the 3′ end of poly(A) RNA is directed towards the catalytic centre of Caf1/CNOT7, thereby providing a rationale for enhanced deadenylation by Caf1/CNOT7 in the presence of BTG2 and PABPC1.

Introduction

BTG2 is a member of the BTG/Tob family of proteins that is conserved in metazoans.[1–3] There are six BTG/Tob proteins in human cells: in addition to BTG2, the family consists of BTG1, which is highly similar to BTG2, the paralogues TOB1 and TOB2, and the more distantly related BTG3 and BTG4 proteins. A common feature of the proteins is their ability to reduce cell cycle progression when overexpressed.[1–3]

The importance of BTG1 and BTG2 in regulating cell proliferation is exemplified by their requirement to maintain T-cell quiescence, a state of low proliferation and cellular metabolism.[4] In the absence of both BTG1 and BTG2, proliferation is increased, and spontaneous T-cell activation occurs. In cancer, recurring missense mutations in BTG1 and BTG2 have been identified in non-Hodgkin lymphoma.[5–8] In diffuse, large B-cell lymphoma, inactivating mutations in BTG1 and BTG2 show a statistically significant overlap,[7] which is

consistent with notion that these very similar proteins can be functionally redundant in certain cell types. Using large whole-exome sequencing data sets of diverse tumour types, BTG2 has been identified as a cancer driver gene in lymphomas.[9] Apart from its role in lymphoma, aberrant expression of BTG2 is observed in several other cancers, including down-regulation of BTG2 in renal and breast cancer.[10–12]

The defining feature of the BTG/Tob family is the presence of the conserved N-terminal BTG domain, which comprises 108–112 amino acids.[1–2,13] This domain mediates the interaction with the Caf1 (CNOT7/CNOT8) catalytic subunit of the Ccr4-Not complex,[14–15] which is involved in the shortening and removal of the poly(A) tail (deadenylation) of mature, cytoplasmic mRNA.[16–18] This step initiates the subsequent removal of the 5′ cap structure by the Dcp1-Dcp2 complex, which exposes the mRNA to 5′-3′ degradation by Xrn1.[19–20] In agreement with the importance of the interaction between BTG/Tob proteins and the Caf1 subunit of Ccr4-Not, several BTG/Tob proteins have been shown to stimulate deadenylation and mRNA degradation.[21–23] Moreover, the ability of BTG2 and TOB1/TOB2 to inhibit cell cycle progression is dependent on their interaction with Caf1 suggesting that this function is mediated by mRNA degradation.[21,24–25]

In addition to their ability to interact with the Ccr4-Not complex, several BTG/Tob proteins can interact with cytoplasmic poly(A) binding protein 1 (PABPC1).[21,23–24,26–27] TOB1 and TOB2 interact with the C-terminal MLLE domain of PABPC1, which is mediated by PAM2 motifs in the extended C-termini of TOB1/TOB2.[21,23,27] While expression of TOB1/TOB2 variants that are unable to interact with PABPC1 fail to stimulate mRNA degradation, this requirement can be by-passed by artificial recruitment of the proteins to mRNA suggesting that the TOB1/TOB2 proteins stimulate mRNA degradation by recruitment of the Ccr4-Not complex.[21,23] More recently, BTG1 and BTG2 were also shown to interact with PABPC1.[24] However, in this case, the interaction is mediated by a short motif, the Box C region, that interacts with the first N-terminal RNA Recognition Motif (RRM1) of PABPC1.[24,26] As is the case for TOB1 and TOB2, a BTG2 variant that is unable to interact with PABPC1 does not inhibit cell cycle progression indicating that both the ability to bind Ccr4-Not and PABPC1 is important for the function of BTG2.[24]

To understand the interaction between BTG2 and PABPC1 in detail, we aimed to identify specific amino acid residues of PABPC1 that are important for binding BTG2. While it was established that BTG2 interacts with the RRM1 domain of PABPC1 via its Box C region,[24] no specific amino acids of RRM1 of PABPC1 were identified. Therefore, we first used a computational approach to predict possible interfaces and identified candidate interaction residues of PABPC1 based on the struc-

ture of the PABPC1 RRM1-RRM2 complex with poly(A) RNA. This was followed by a mutagenesis approach to identify the involvement of specific residues of PABPC1 required for the interaction with BTG2, but not interfering with poly(A) binding. After these experiments were completed, the mapping of interacting residues of both BTG2 and PABPC1 by NMR chemical shift perturbation experiments was reported.[26] We used this information as ambiguous interaction restraints for data-driven docking[28–29] and applied our mutagenesis data to validate the docking results. The resulting structural model of the BTG2-PABPC1 complex provides a rationale for enhanced deadenylation of PABPC1-poly(A) RNA by Caf1/CNOT7 in the presence of BTG2.

Materials and methods

Prediction of macromolecular interaction surfaces

For the prediction of interaction surfaces of human PABPC1, the CPORT webserver (https://milou.science.uu.nl/services/CPORT/) was used,[30] which integrates the output of six algorithms: WHISCY,[31] ProMate,[32] SPPIDER,[33] PINUP,[34] PIER[35] and cons-PPISP.[36] PDB structure 4F02 (chain A) of human PABPC1 in complex with poly(A) and eIF4G and the corresponding HSSP alignment were used as input using the "very sensitive" threshold setting.[37] PABPC1 residues involved in the binding of poly(A) RNA and eIF4G were identified using the PISA webserver (https://www.ebi.ac.uk/pdbe/pisa/).[38]

Plasmids and recombinant DNA techniques

Plasmid pQE80L-PABPC1 (1–190) containing a hexa-histidine tag in-frame with a cDNA encoding human PABPC1 (amino acids 1–190) was described before.[39] Plasmid pGEX4-T1-BTG2 for the expression of a GST-human BTG2 fusion protein was also described before.[40] Site-directed mutagenesis was carried out using either a modified Quickchange protocol, or using inverse PCR using Phusion High-Fidelity DNA polymerase (NEB). Complete cDNA sequences were confirmed by Sanger DNA sequencing (Source Biosciences).

His-pulldown interaction analysis

Human His-PABPC1 and human GST-BTG2 were expressed in *Escherichia coli* strain BL21 (DE3) by transformation of the cells using plasmid pQE80L-PABPC1 (1–190) or pGEX4-T1-BTG2. Cultures (50 ml) were grown at 37 °C until OD₆₀₀ reached 0.6–0.8. Then, protein expression was induced by the addition of isopropyl-β-D-1-thiogalactopyranoside (IPTG, 0.2 mM final concentration) and incubation was continued for 3 h at 30 °C. Cells expressing GST-BTG2 were harvested by centrifugation at 4,000 rpm for

30 min and lysed in 20 mM Tris-HCl pH 7.8, 300 mM NaCl, 5% glycerol and 1 mM β-mercaptoethanol. Cells expressing His-PABPC1 (1–190) were lysed in 20 mM Tris-HCl pH 7.8, 300 mM NaCl, 5% glycerol, 1 mM β-mercaptoethanol, 0.1% NP-40, and 40 mM imidazole. Lysed cultures were sonicated for 5 min using 10 sec on/off cycles and centrifuged at 10,000 rpm for 30 min at 4 ℃ using an Eppendorf 5810R centrifuge (rotor FA-45–48-11). Clarified lysates containing His-PABPC1 variants were mixed with lysates containing GST-BTG2 and Ni-NTA magnetic beads (Pierce, cat no 78605) for 1 h at 4 °C. After separating the beads using a magnetic separation stand (Magnesphere, Promega), beads were washed three times with a solution containing 20 mM Tris-HCl pH 7.8, 300 mM NaCl, 5% glycerol and 1 mM β-mercaptoethanol, 0.1% NP-40, and 40 mM imidazole. Bound proteins were then eluted using a solution containing 20 mM Tris-HCl pH 7.8, 300 mM NaCl, 5% glycerol and 1 mM β-mercaptoethanol, 0.1% NP-40, and 200 mM imidazole, separated using 15% SDS-PAGE, and stained with Coomassie Brilliant Blue.

Protein expression and purification

His-PABPC1 (1–190) was expressed and purified from *E. coli* BL21 (DE3) using plasmid pQE80L-PABPC1 (1–190) essentially as described previously.[39] Briefly, after metal affinity purification using a 1 mL HiTrap Talon pre-packed column (Cytiva), peak fractions were pooled and buffer was adjusted to buffer SA (20 mM Tris-HCl pH 7.8, 250 mM NaCl, 10% glycerol, 2 mM β–mercaptoethanol) using PD-10 gravity flow columns (Cytiva). Protein concentrations were determined using the Protein Assay Reagent (Bio-Rad). Purified proteins were stored in small aliquots at −80 °C and confirmed to be free of ribonuclease activity.

The monomeric human Caf1/CNOT7 enzyme was expressed and purified from *E. coli* BL21 (DE3) using expression plasmid pQE80L-CNOT7 as described before[40]. The BTG2-CNOT7 dimer was expressed and purified as described before using plasmid pACYC-Duet1-BTG2/CNOT7 for dual expression of BTG2 and CNOT7.[39] Purified proteins were stored in small aliquots at −80 °C. Protein concentrations were determined using the Protein Assay Reagent (Bio-Rad).

RNA electrophoretic mobility shift assay

5′-Flc-labelled poly(A)$_{20}$ RNA (0.2 μM) (Sigma-Genosys) was incubated with the indicated molar excess of purified PABPC1 (amino acids 1–190) variants for 15 min at room temperature in 20 mM Tris-HCl pH 7.9, 50 mM NaCl, 2 mM MgCl$_2$, 10% glycerol, 1 mM β–mercaptoethanol (10 μl). After addition of 2 μl native loading dye (0.05% bromophenol blue, 0.05% xylene cyanol, 25% glycerol in 1 × TBE), 6 μl of the mixture was analysed by electrophoresis using an 8% polyacrylamide:bisacrylamide (19:1) gel cast and run in 1 × TBE at 120 V for 50–60 min. RNA was visualised using epi-fluorescence using a Fujifilm LAS-4000 instrument.

Deadenylase assays

Standard reactions (25 μl final volume) contained 100 nM enzyme, 20 mM Tris-HCl pH 7.9, 50 mM NaCl, 2 mM MgCl$_2$, 10% glycerol, 1 mM β-mercaptoethanol and 0.2 μM 5′-Flc-labelled RNA substrate (Sigma-Genosys) in nuclease-free water. 5′-Flc-labelled poly(A)$_{20}$ RNA was incubated with an 8-fold excess of purified PABPC1 (amino acids 1–190) variants for 15 min at room temperature in 20 mM Tris-HCl pH 7.9, 50 mM NaCl, 2 mM MgCl$_2$, 10% glycerol, 1 mM β–mercaptoethanol. After addition of CNOT7 enzyme or the CNOT7-BTG2 complex, reactions were incubated at 30 ℃ for the indicated amount of time. Reaction products were analysed by denaturing 20% polyacrylamide gel electrophoresis.[39] Gel images were obtained using epi-fluorescence using a Fujifilm LAS-4000 instrument.

Data-driven docking

The HADDOCK 2.4 webserver (https://wenmr.science.uu.nl/haddock2.4) was used for modelling the PABPC1-BTG2 complex using default settings.[29,41] Twenty-seven ambiguous interaction restraints (active residues) were defined based on NMR perturbation experiments described by Amine *et al.*[26] (Table 1). The structures of PABPC1 (4F02, chain A)[37] and BTG2 (3DJU, chain B)[15] were used for docking. Passive residues were automatically assigned. In brief, 1000 structures were calculated for rigid body docking. The 200 structures with the best HADDOCK scores were then refined by semi-flexible simulated annealing and water refinement. After water refinement, the 200 docking solutions were clustered using the fraction of common contacts, a cut-off of 0.6, and minimum number of structures per cluster of 12. Structures were visualised using PyMOL.[42]

Results

Prediction of residues of PABPC1 that are required for binding BTG2

To determine how RRM1 of PABPC1 is involved in the interaction with BTG2,[24] we set out to identify specific residues of RRM1 of PABPC1 that are required for the interaction. First, we used a computational approach to identify candidate residues in PABPC1 RRM1-RRM2 using the CPORT tool,[30] which predicts possible interaction residues based on six different algorithms.[31–35,43] We then used the PISA webserver[38] to identify known interaction

Table 1 Ambiguous interaction restraints.

Protein	Residues[a]
PABPC1	Glu–24, Ala–25, Leu–27, Glu–29, Lys–30, Arg–41, Val–42, Cys–43, Arg–44, Asp–45, Tyr–56, and Lys–78
BTG2	Leu–23, Thr–26, Ser–110, Tyr–111, Arg–112, Ile–113, Gly–114, Glu–115, Asp–116, Gly–117, Ser–118, Ile–119, Cys–120, Val–121, Leu–122

[a] Ambiguous interaction restraints were selected using NMR chemical shift perturbations; $\Delta\delta$ (^{1}H, ^{15}N) > 0.18 ppm (PABPC1) and $\Delta\delta$ (^{1}H, ^{15}N) > 0.14 ppm (BTG2). Data were obtained from Amine *et al.*[26].

residues of PABPC1 RRM1-RRM2 involved in the binding with poly(A) RNA[37] and compared the predicted and known set of interaction residues to evaluate the accuracy of the algorithms (Figure 1). In total, 38 possible interaction residues of PABPC1 RRM1-RRM2 were identified, which included the majority of the known interacting residues of PABPC1 with poly(A) RNA (Figure 1) (**Supplementary Table S1**). In addition, a region at the tip of RRM1 was predicted to form a possible macromolecular interaction region. This region included residues Asp-21 and Glu-24 located in the region following β-strand β1 and α2, and residues Met-46, Thr-48, Arg-49, and Arg-50 in the region between β2 and β3. Because it was shown that PABPC1 RRM1-RRM2 can form a ternary complex with poly(A) RNA and BTG2,[24] we hypothesised that this region, which is not involved in RNA binding, may be involved in the interaction between PABPC1 RRM1 and BTG2.

Confirmation of PABPC1 residues required for the interaction with BTG2

To confirm the involvement of the predicted interaction region in the binding of BTG2, we carried out pulldown assays using wild type PABPC1 RRM1-RRM2 (1–190) and PABPC1 variants containing single amino acid substitutions in RRM1 (Figure 2(**A**)). In addition to residues identified through the computational approach, we also included additional residues that were located in close vicinity (Figure 1(**B**)). After expressing His-PABPC1 variants and GST-BTG2 in *E. coli*, soluble lysates were mixed followed by pulldown of His-PABPC1 variants and interacting GST-BTG2. This analysis showed that PABPC1 variants D21A and E29A were able to bind GST-BTG2 similarly to wild type PABPC1. By contrast, variants E24A, I40A, R44A, M46A, R49A, R50A, and R49E displayed reduced or no binding to GST-BTG2 (Figure 2(**A**)).

Interrogation of the catalogue of somatic mutations in cancer (COSMIC) revealed that rare mutations in PABPC1 are found in various tumour types (Figure 2(**B**)).[44] A common recurring mutation in PABPC1, resulting in amino acid substitution T48P, was found in > 24 different head and neck, thyroid and oesophageal cancer samples. Because this mutation causes an amino acid substitution in the region of PABPC1 that is involved in the interaction with BTG2, we analysed the interaction between the two PABPC1 variants and GST-

BTG2 using the His pulldown assay (Figure 2(**C**)). This analysis showed that the variant T48A has a similar ability to interact with GST-BTG2 as wild type PABPC1. By contrast, the cancer-associated variant T48P displayed a reduced ability to bind GST-BTG2.

In summary, our data demonstrate that PABPC1 residues Glu-24, Ile-40, Arg-44, Met-46, Thr-48, Arg-49, and Arg-50 are involved in the interaction with BTG2.

The PABPC1 variants R49E and T48P both bind poly(A) RNA, but PABPC1 R49E is unable to stimulate deadenylation by BTG2-CNOT7

Next, we investigated whether PABPC1 variants T48P and R49E retained the ability to bind poly(A) RNA (Figure 3). To this end, wild type His-PABPC1 (1–190) and variants T48P and R49E were expressed in *E. coli* and purified using immobilised metal-affinity purification (Figure 3(**A**)). Purified PABPC1 variants were incubated with 5′ fluorescein-labelled A$_{20}$ and PABPC1-poly (A) complexes were analysed by electrophoretic mobility shift assays (Figure 3(**B**)). As evident from the formation of PABCP1-RNA complexes, PABPC1 variants T48P and R49E retained the ability to bind poly(A) to a similar extent as wild type PABPC1 (1–190) (Figure 3(**C**)).

We then assessed the impact of amino acid substitutions T48P and R49E in PABPC1 on their ability to stimulate deadenylation by Caf1/CNOT7 in the absence or presence of BTG2. Therefore, we expressed and purified the Caf1/CNOT7 nuclease as well as BTG2-Caf1/CNOT7 complexes (Figure 3(**D**)). Prior to addition of the nuclease, purified PABPC1 (1–190) was incubated with poly(A) RNA to allow the formation of PABPC1-poly(A) complexes. Upon addition of Caf1/CNOT7, deadenylation was barely detectable under the conditions used (Figure 3(**E**)), which is in agreement with our previously published data.[39] By contrast, deadenylation was readily observed under the same conditions in the presence of the BTG2-Caf1/CNOT7 dimer (Figure 3(**E**)).[39] In the presence of the cancer-associated PABPC1 variant T48P, a similar level of deadenylation was observed as compared to wild type PABPC1. This suggests that the residual ability of the T48P PABPC1 variant to bind BTG2 is sufficient to stimulate deadenylation by the BTG2-Caf1/CNOT7 dimer. By contrast, in the presence of PABPC1 R49E, a substantial decrease in dead-

Figure 1. Predicted interaction residues of PABPC1 involved in protein:protein or protein:RNA binding. (A) Structure of human PABPC1 RRM1-RRM2 (*light grey*) in complex with poly(A) RNA (*blue*) (PDB 4F02).[37] Predicted interaction residues were identified using the CPORT algorithm.[30] *Yellow*, predicted interaction residues without known binding partner, *violet*, predicted interaction residues involved in RNA binding, *dark purple*, RNA interaction residues not identified using CPORT. (B) Alignment of RRM1 residues of PABPC1 orthologues from human (*Hs*), mouse (*Mm*), fission yeast (*Sp*) and budding yeast (*Sc*). Secondary structure elements are indicated based on the human PABPC1 structure.

enylation by BTG2-Caf1/CNOT7 was observed (Figure 3(**E**)). This is in agreement with the observation that the PABPC1 R49E variant was unable to bind BTG2.

Amino acid residues of BTG2 required for binding PABPC1

Having identified several interfacing residues of PABPC1 required for the interaction with BTG2, we aimed to define in more detail which residues of BTG2 are important for the interaction with PABPC1. To confirm the involvement of Box C residues of BTG2 (amino acids 117–126) in the interaction with RRM1 of PABPC1,[24] we first evaluated two BTG2 variants (Figure 4(**A**)). When Box C

residues were removed (BTG2Δ117-126), no interaction between His-PABPC1 and GST-BTG2 was observed. By contrast, when a stop codon was introduced immediately after Box C (BTG2 1– 126), a similar level of BTG2 was pulled down as compared to wild type GST-BTG2 (Figure 4(**A**)). This indicates that residues C-terminal from Box C do not contribute significantly to the interaction with PABPC1.

Next, we compared Box C residues of BTG2, and the corresponding residues in TOB1 and TOB2, which share structural similarity in this region, but do not interact with PABPC1 RRM1 through this region (Figure 4(**B**)) (**Supplementary Figure S1**). Alteration of amino acid Ser-118 and Ile-119 of BTG2 to the corresponding residues of TOB2

Figure 2. Confirmation of residues required for the interaction between PABPC1 and BTG2. (A) Residues of PABPC1 required for interaction with BTG2. (*Top panel*) Lysates containing wild type GST-BTG2 or His-PABPC1 (amino acid 1–190) variants used as input for pulldown assays. (*Bottom panel*) Analysis of bound proteins following His-pulldown analysis. (B) Schematic diagram of human PABPC1 and cancer-associated variants. Selected PABPC1 mutations in cancer were identified through the catalogue of somatic mutations in cancer (COSMIC) v90 (https://cancer.sanger.ac.uk/cosmic).[44] (C) Reduced interaction between PABPC1 (1–190) T48P and BTG2. (*Left panel*) Lysates containing wild type GST-BTG2 and His-PABPC1 (amino acid 1–190) variants. (*Right panel*) Analysis of bound proteins following His-pulldown analysis. Proteins were separated by 14% SDS-PAGE and stained with Coomassie Brilliant Blue.

(S118A/I119V) disrupted the interaction with PABPC1 even though BTG2 containing the single substitutions S118A or I119V was able to bind PABPC1 (Figure 4(C)). Similarly, substitution of residue 124 or 125 with alanine (E124A or E125A) did not interfere with the interaction, but substitution of BTG2 residues 124–126 with the corresponding residues of TOB2 (E124L/E125D/A126D) abrogated the interaction with PABPC1 (Figure 4(C)).

Structural model of the PABPC1-BTG2 complex using information-driven docking

While this manuscript was in preparation, the mapping of interfacing residues of both PABPC1 and BTG2 using NMR chemical shift perturbation analysis was reported.[26] The identified residues using the NMR approach showed overlap with, but were not identical to, the residues identified using our approach (Supplementary Figure S2). For

example, Arg-49 of PABPC1 was not identified by NMR chemical shift perturbation analysis of backbone atoms, which may be due to the long side chain of Arg-49 of PABPC1. We reasoned that we could derive a structural model of the BTG2-PABPC1 complex by using the data set of Amine *et al.*[26] for NMR-guided docking in combination with our mutagenesis data. Thus, based on the reported changes in chemical shifts by Amine *et al.*,[26] we defined twelve ambiguous interaction restraints for PABPC1 and fifteen for BTG2 (Table 1).

The ambiguous interaction restraints were then used in combination with the structures of PABPC1 and BTG2 to derive a structural model of the complex using the High Ambiguity Driven biomolecular DOCKing (HADDOCK) package.[28–29] Four clusters of solutions contained more than 12 structures each and represented 62.5% (125/200) of all solutions (Table 2). Cluster 2 had the best statistics, i.e. best HADDOCK score, smallest deviation from the overall lowest-energy solu-
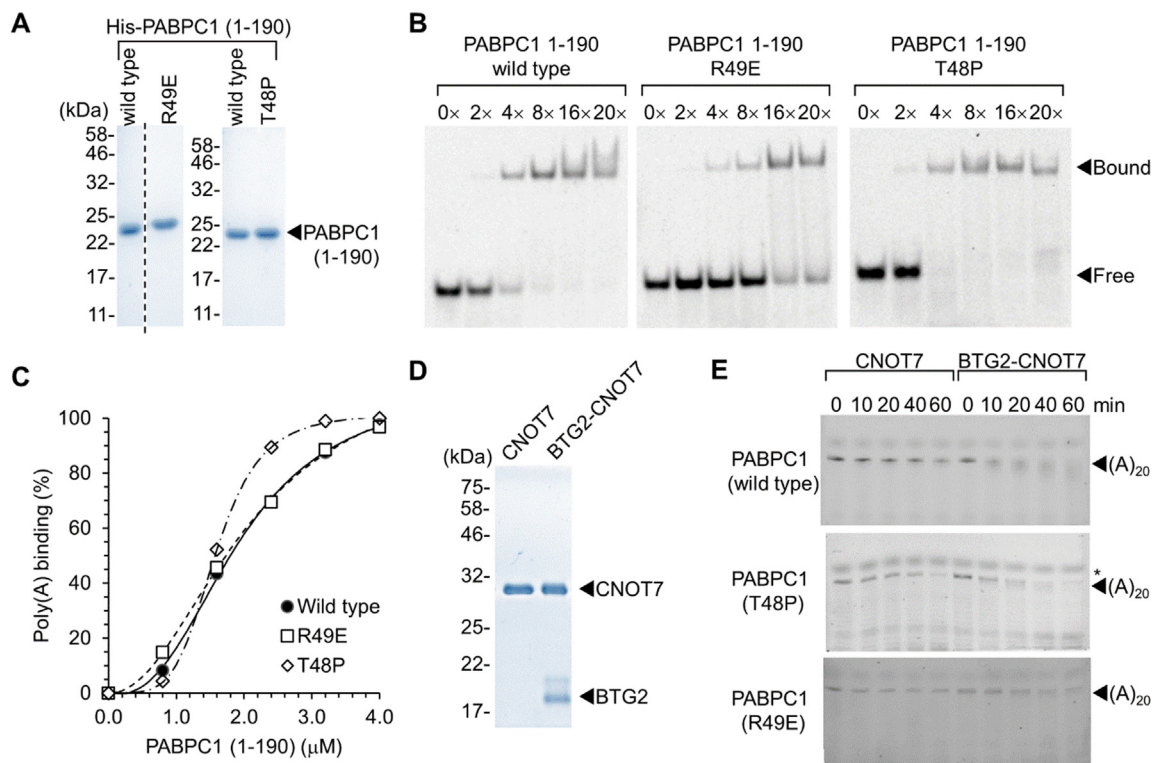
Figure 3. Poly(A)-RNA binding by PABPC1 with reduced ability to interact with BTG2. (A) Purified PABPC1 (amino acid 1–190) proteins. Proteins were separated by 14% SDS-PAGE and stained with Coomassie Brilliant Blue. The left panel shows two lanes from the same gel. (B) Poly(A) binding by wild type PABPC1 (1–190) (*left*), PABPC1 (1–190) T48P (*middle*) and PABPC1 (1–190) R49E (*right*). Fluorescein-labelled $(A)_{20}$ RNA oligonucleotides were incubated with PABPC1 proteins using the indicated molar ratios. RNA and RNA:PABPC1 complexes were subsequently separated by 8% polyacrylamide:bisacrylamide gel electrophoresis. (C) Quantitative analysis of poly(A) binding by wild type PABPC1 (1–190), and variants T48P and R49E. Data were obtained from densitometric analysis of EMSA experiments (*n* = 3). (D) Purified Caf1/CNOT7 and BTG2-Caf1/CNOT7 complex. Proteins were separated by 14% SDS-PAGE and stained with Coomassie Brilliant Blue. (E) Deadenylation of poly(A):PABPC1 substrates by Caf1/CNOT7 and the BTG2-Caf1/CNOT7 complex in the presence of wild type PABPC1 (1–190), PABPC1 (1–190) T48P and PABPC1 (1–190) R49E. Purified Caf1/CNOT7 or BTG2-Caf1/CNOT7 (0.1 μM) was incubated with 0.2 μM fluorescein-labelled $(A)_{20}$:PABPC1 substrate and incubated at 30°C for the incubated time. RNA was separated by 50% urea:20% PAGE.

tion, largest buried surface, and largest electrostatic energy contribution (Table 2, Figure 5(**A**)). In the lowest energy solution of cluster 2, residues of PABPC1 identified using NMR chemical shift perturbation analysis form a continuous interface with the exception of Tyr-56 and Lys-78, which are more closely located to the poly(A) interaction surface (Figure 5(**B**), (**C**)).

To evaluate which solution(s) were in agreement with the mutational analysis, we first assessed the position of Arg-49 of PABPC1, which was not identified as significantly perturbed in NMR titration experiments and therefore not used as an ambiguous restraint. In the best scoring solutions of cluster 2, Arg-49 of PABPC1 forms a network of electrostatic interactions with the backbones of Leu-122 and Glu-124 of BTG2 (Figure 5(**D**), **Supplementary Figure S3**). In this solution, the E124L substitution of BTG2 cannot be

accommodated due to steric clashes, explaining why the EEA → LDD substitution of residues 124–126 of BTG2 disrupts the interaction between BTG2 and PABPC1 (Figure 4(**C**)).

In cluster 1, which has a significantly higher energy score compared to cluster 2, Arg-49 of PABPC1 does not make any inter-chain contacts even though residue Glu-124 of BTG2 forms a hydrogen bond with Lys-78 of PABPC1 (**Supplementary Figure S3**). Thus, cluster 1 is not consistent with the mutagenesis data. In cluster 3, Arg-49 of PABPC1 is involved in hydrogen bonding with residue Ser-98 of BTG2, while, in cluster 4, Arg-49 of PABPC1 forms contacts with the sidechain of Asp-116 of BTG2. However, for both clusters 3 and 4, residues Glu-124, Glu-125, and Ala-126 of BTG2 do not form any interactions with PABPC1 and the solutions in these clusters are therefore not consistent with the
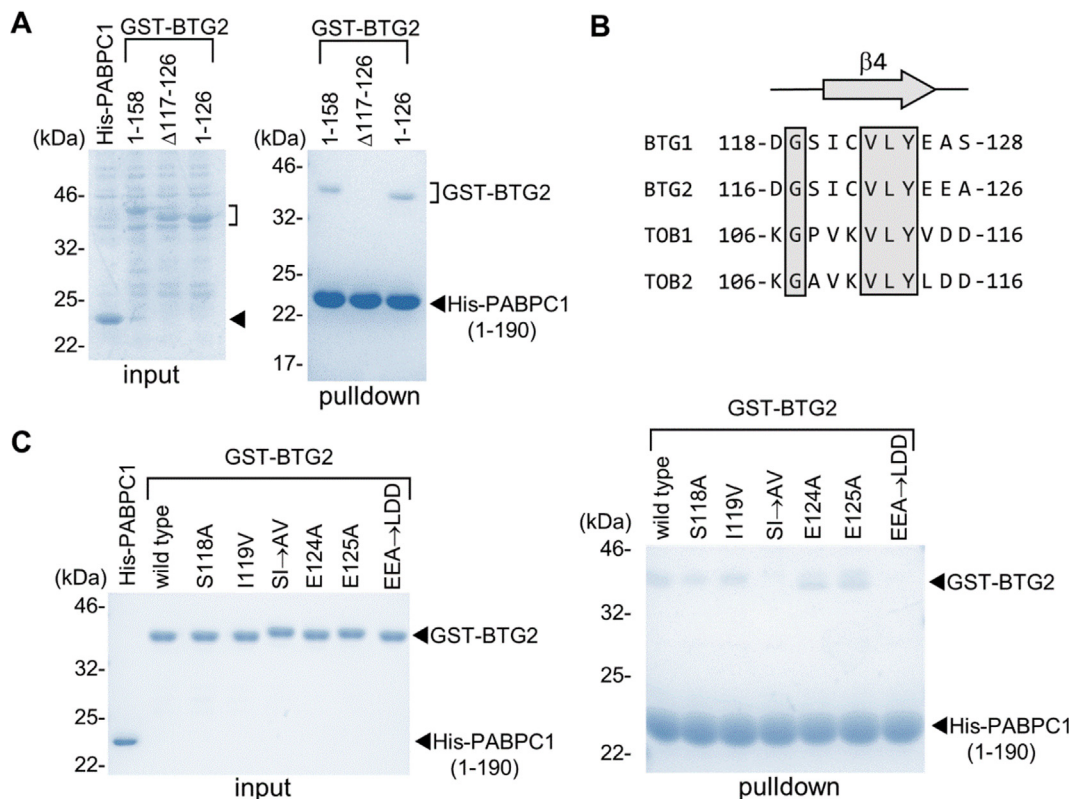
Figure 4. Amino acid residues of BTG2 required for binding with PABPC1 (1–190). (A) Identification of residues of BTG2 involved in binding to PABPC1. (*Left*) Lysates containing wild type His-PABPC1 (amino acid 1–190) or wild type GST-BTG2 (amino acids 1–158), GST-BTG2 lacking the Box C sequence (Δ116-126), or GST-BTG2 containing a stop codon following the Box C sequence (1–126). (*Right*) Analysis of bound proteins following His-pulldown analysis of PABPC1 (1–190). (B) Comparison of Box C sequences of BTG1 and BTG2 and the corresponding regions of TOB1 and TOB2. Residues of BTG2 forming β-strand 4 (β4) are indicated. (C) Identification of residues of Box C residues of BTG2 involved in binding to PABPC1. (*Left*) SDS-PAGE analysis of purified wild type His-PABPC1 (amino acid 1–190) or the indicated GST-BTG2 variants. (*Right*) Analysis of bound proteins following His-pulldown analysis of PABPC1 (1–190). Proteins were separated by 14% SDS-PAGE and stained with Coomassie Brilliant Blue.

mutagenesis data (**Supplementary Figure S3**). Thus, in addition to having the lowest energy and the smallest deviation from the overall lowest-energy solution, cluster 2 is also the only cluster consistent with the mutagenesis data.

In cluster 2, in addition to a network of polar interactions between Arg-49 of PABPC1 and Leu-122, Glu-124 and Glu-125 of BTG2, extensive hydrogen bonding is observed between Glu-24 of PABPC1 and Tyr-111 of BTG2, Tyr–28 of PABPC1 and the backbone of Ile-113 of BTG2, side-chain interactions between Glu-29 of PABPC1 and Arg-27 of BTG2, backbone interactions between Leu-38 of PABPC1 and Ile-119 of BTG2, and sidechain interactions between Lys-78 of PABPC1 and Thr-26 of BTG2 (**Supplementary Figure S3**). In addition to polar contacts, Van der Waals interactions are present between Thr–23 and Ala–25 of PABPC1 and Leu–23, Ser–22, and Phe–19 of BTG2, as well as Ser–39 and Ile–40 of PABPC1 and Ser–118 of BTG2 (**Supplementary Figure S3**).

Based on alanine scanning analysis, six residues of PABPC1 were shown to affect the interaction with BTG2. In cluster 2, Glu-24, Ile-40, Arg-44, and Met-46 are located on the interface of PABPC1. As mentioned above, Glu-24 and Ile-40 of PABPC1 are involved in hydrogen binding and Van der Waals interactions, respectively. Arg-44 of PABPC1 may form Van der Waals interactions with Leu-122 of BTG2, while Met-46 forms Van der Waals bonds with the backbone linking Glu-124 and Glu-125 of BTG2. Arg-50 and Thr-48 of PABPC1 are not located on the interface with BTG2. However, the sidechains of these residues may form hydrogen bonds and stabilise the secondary structure around Arg-49 thereby indirectly contributing to the interaction with BTG2.

Quaternary poly(A)-PABPC1-BTG2-CNOT7 complex

To obtain insight into the mechanism by which BTG2 enhances deadenylation of poly(A)-

Table 2 Structure statistics of the top-4 clusters representing 125 water-refined models (62.5% of all models).

Cluster	Score	Cluster size (n)	RMSD[a] (Å)	Buried surface area (Å²)	Van der Waals energy (kcal/mol)	Electrostatic energy (kcal/mol)	Desolvation energy (kcal/mol)	Restraints violation energy (kcal/mol)
1	−79.0 ± 3.2	46	14.5 ± 0.1	1610 ± 74	−44.0 ± 2.3	−271.4 ± 23.9	10.4 ± 2.7	88.2 ± 19.2
2	−101.2 ± 2.4	45	0.5 ± 0.3	1655 ± 53	−46.1 ± 1.9	−360.2 ± 21.2	9.9 ± 1.6	70.7 ± 12.1
3	−73.6 ± 4.9	21	14.4 ± 0.3	1337 ± 49	−28.4 ± 3.9	−316.3 ± 25.4	10.5 ± 3.2	76.2 ± 7.2
4	−78.7 ± 9.0	13	11.2 ± 0.3	1370 ± 95	−48.5 ± 6.6	−229.5 ± 32.0	10.9 ± 0.8	48.1 ± 17.2

[a] The root mean square deviation (RMSD) compared to the overall lowest-energy solution.

PABPC1 by Caf1/CNOT7, we next constructed a model of the quaternary poly(A)-PABPC1-BTG2-Caf1/CNOT7 complex. This was achieved by superimposing the X-ray structures of poly(A)-PABPC1 (PDB 4F02)[37] and TOB1-Caf1/CNOT7 (PDB 2D5R)[14] with the model of the BTG2-PABPC1 complex (Figure 6). In the quaternary model, the 3′ end of poly(A) bound to PABPC1 is directly oriented towards the active site residues of CNOT7, which degrades the poly(A) tail in a 3′-5′ direction. It can thus be conceived that extending the 3′ poly(A) residues would position Caf1/CNOT7 in an orientation that would promote deadenylation. This model provides a structural view of the proposed mechanism of enhanced deadenylation by Caf1/CNOT7 in presence of PABPC1 and BTG2, and provides insight into a general mechanism of recruitment of Ccr4-Not to the mRNA poly(A) tail.

Discussion

The BTG2 protein is a general activator of mRNA deadenylation that stimulates degradation of the poly(A) tail by Ccr4-Not by connecting the catalytic subunit Caf1/CNOT7 and PABPC1.[22,24] In this work, we identified a critical residue, Arg-49 of PABPC1, that is required for the interaction with BTG2. This residue was identified using an initial bioinformatics approach, which reduced the amount of resources required for validation. The identification of Arg-49 had two implications. First, it led to the discovery of the R49E substitution, which allows to distinguish between the roles of PABPC1 in BTG2 and poly(A) binding. Secondly, it contributed to the validation of a structural model of the BTG2-PABPC1 complex obtained using data-driven docking using NMR chemical shift perturbation data.[26]

Amino acids of PABPC1 required for specific interactions

In order to understand the BTG2-PABPC1 interaction in more detail, we started this work by identifying possible residues of PABPC1 involved in macromolecular interactions using a bioinformatics approach. The prediction of amino acids involved in protein–protein, or protein-RNA interactions can have limitations, as exemplified by the fact that eIF4G interacting residues of PABPC1 were not identified. On the other hand, the combined use of six prediction algorithms[30–33,35–36] identified most PABPC1 residues involved in poly(A) binding, indicating that this approach can result in useful information. Indeed, this method resulted in the identification of Arg–49 as a key residue of PABPC1 on the interface with BTG2. Even though this approach has limitations, it can therefore be used to identify interfacing residues with relatively limited experimental resources as compared to alternative strategies involving, for example, the screening of libraries created by random mutagenesis.

The residues identified in the bioinformatic approach rely, amongst other criteria, on sequence conservation. It is therefore expected that many residues identified using this method were conserved from yeast to human even though the yeasts S. cerevisiae and S. pombe do not contain orthologue(s) of BTG1/BTG2. It is worth noting, however, that most residues of PABPC1 predicted to interact with BTG2 were not invariant unlike most residues involved in RNA binding (Figure 1(B)).

A structural model of the BTG2-PABPC1 complex

The structural model of the BTG2-PABPC1 complex presented here was derived by molecular docking using ambiguous interaction restraints obtained from NMR chemical shift perturbation mapping described by Amine *et al.*[26] Interestingly, Arg–49 of PABPC1 was not identified in this experiment, which could be explained if the interactions involving this residue were mediated by its long side chain, and therefore did not result in backbone chemical shift perturbations. Because this residue was not used as an ambiguous interaction restraint, it provided an independent way to validate the docking solutions. In addition, we used information derived from BTG2 mutagenesis experiments involving the replacement of Box C residues of BTG2 with the corresponding residues of TOB2, which does not interact with PABPC1 via this region. Only one cluster, the second largest and the cluster with the lowest deviation from the overall lowest energy solution, was consistent with the mutagenesis data.
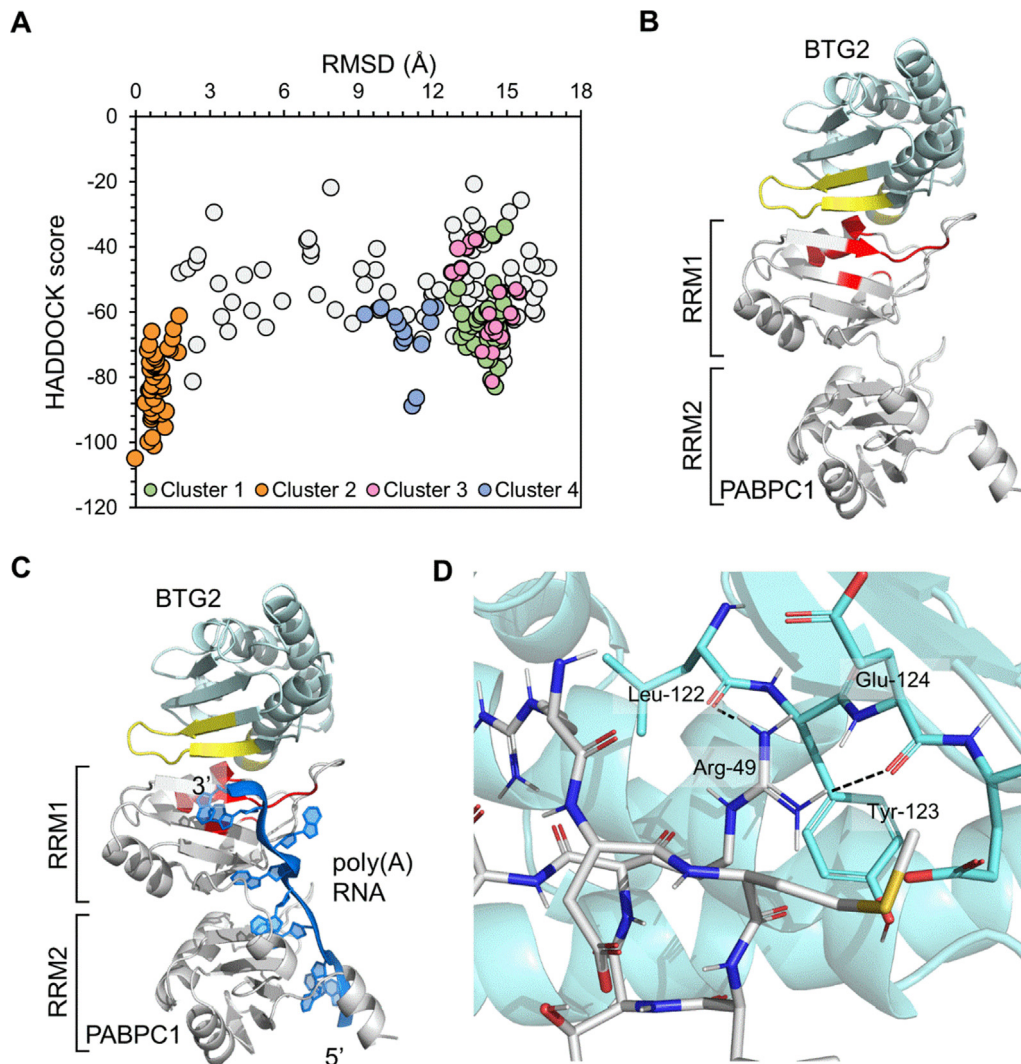
Figure 5. Information-driven modelling of a PABPC1-BTG2 complex. (A) Overview of the docking solutions obtained using HADDOCK.[29] Solutions were clustered using the fraction of common contacts and displayed according to the root mean square deviation compared to the lowest overall solution. (B) Best solution of cluster 2 of the BTG2 – PABPC1 complex. Highlighted are: active residues (*yellow*) of BTG2 (*light cyan*),active residues (*red*) of PABPC1 (*white*) used for information-driven docking. (C) Superposition of the PABPC1-BTG2 model with a PABPC1-poly(A) structure (PDB 4F02).[37] Poly(A) RNA is indicated in blue. (D) Interactions between Arg–49 of PABPC1 with backbone residues of Leu-122 and Glu-124 of BTG2.

Interestingly, BTG1 and BTG2 are not the only BTG/Tob proteins that can interact with PABPC1. The paralogues TOB1 and TOB2 also bind PABPC1, but interact via their PAM2 motifs that are present in their extended C-terminal regions.[21,23] In addition to using different motifs, BTG1/BTG2 and TOB1/TOB2 also interact with different regions of PABPC1. Whereas BTG1 and BTG2 bind RRM1 of PABPC1,[24] which recognises the 3′ end of bound poly(A), TOB1 and TOB2 interact with the C-terminal MLLE (PABC) domain of PABPC1.[21,23] While the functional outcome of the BTG1/BTG2 and TOB1/TOB2 interactions with PABPC1 may be similar, it could also be envisaged that the alternative mode of recruitment results in

differential regulation of deadenylation by BTG1/BTG2 and TOB1/TOB2. The structural model presented here is a further step towards understanding regulated deadenylation at the molecular level, that may help to resolve this and related questions. The use of PABPC1 R49E variant, which has impaired BTG2 binding while keeping is ability to interact with poly(A) similarly to wild type PABPC1, may also be a useful tool towards this end.

It was shown that the Caf1 (CNOT7/CNOT8) and Ccr4 (CNOT6/CNOT6L) subunits of Ccr4-Not have differential roles in deadenylation.[45–46] In the presence of poly(A)-binding protein, the Caf1 subunit is unable to carry out productive deadenylation, whereas Ccr4 is active on poly(A) tails containing
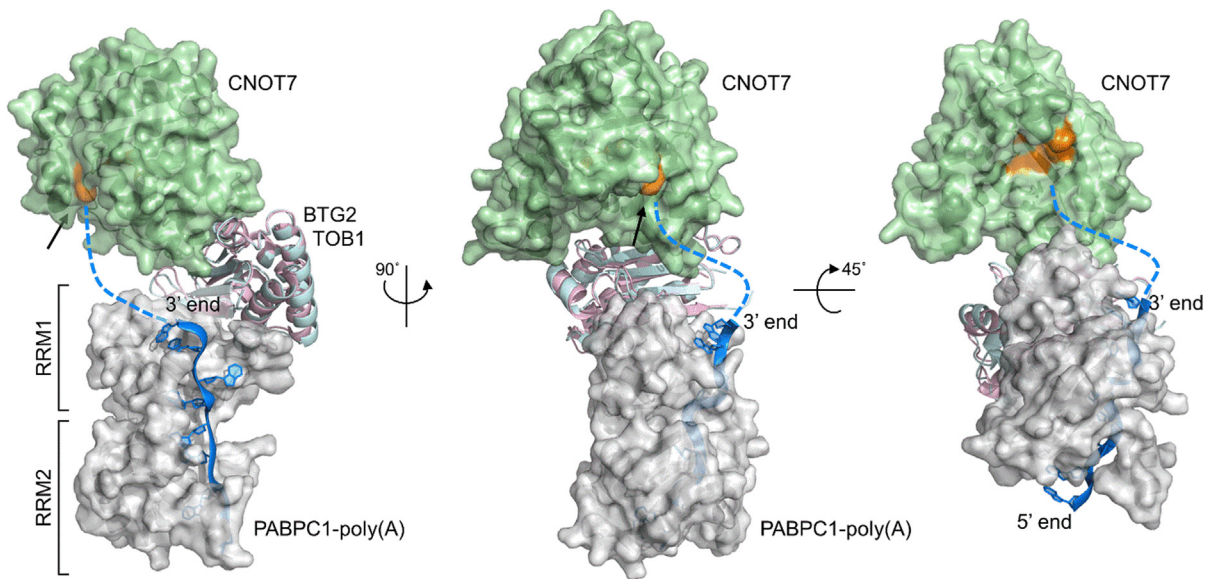
Figure 6. Model of a poly(A)-PABPC1-BTG2-Caf1/CNOT7 quaternary complex. The model was created by superposition of the PABPC1-BTG2 complex, the PABPC1-poly(A) structure (PDB 4F02)[37] and the structure of TOB1 in complex with Caf1/CNOT7 (PDB 2D5R).[14] Indicated are PABPC1 (*white*),BTG2 (*light blue*),TOB1 (*plum*); Caf1/CNOT7 (*light green*); and poly(A) RNA (*blue*). Highlighted (*orange, black arrow*) are the active site residues of Caf1/CNOT7 (Asp-40, Glu-42, Asp-161, His-225, and Asp-230).

poly(A)-binding protein. This appears to be contradictory to the observation that BTG2 can stimulate Caf1/CNOT7-mediated deadenylation of PABPC1-poly(A) substrates.[24] A possible explanation could be that yeast cells do not contain an orthologue of BTG2. In addition, in many immortalised human cell lines, BTG2 appears to be downregulated. Thus, BTG2 -and its paralogue BTG1- may have a regulatory role in activating Caf1-mediated deadenylation of poly(A) bound by PABPC1.

An alternative, but not mutually exclusive, explanation may be that PABPC1 recruits the Caf1 subunit to deadenylate the free, unbound terminal end of the poly(A) tail. In this scenario, the terminal residues at the 3′ end are not bound by PABPC1 and poly(A) would be available for deadenylation by Caf1. Based on our recent model of the nuclease module,[47] the Ccr4 subunit is not placed close to the 3′ end of the poly(A) tail when the complex is bound to PABPC1 via BTG2 (**Supplementary Figure S4**). However, recruitment of Ccr4-Not via the PABPC1-BTG2 interactions may position the 3′ end of the poly(A) tail close to the Ccr4 catalytic domain if the PABPC1 protein bound by BTG2 was distal to the 3′ end, e.g. when the PABPC1 molecule bound by BTG2 is not the protein most proximal to the 3′ end.

The role of BTG2 in cell proliferation and lymphoma

A characteristic of the BTG1/BTG2 paralogues is their ability to reduce cell cycle progression when overexpressed in cell lines.[1–3] The interaction between BTG2 and Caf1 is required for the ability

of BTG2 to inhibit cell proliferation under these conditions.[24–25] Similarly, the interaction between BTG2 and PABPC1 is necessary for the inhibition of cell cycle progression mediated by overexpression of BTG2 in cell lines.[24] This suggests that PABPC1-BTG2-Caf1 act as a functional unit in the regulation of cell proliferation.

In normal tissue, this is exemplified by the role of BTG1 and BTG2 in the regulation of T-cell quiescence.[4] In T-cells, BTG1 and BTG2 are highly expressed in the quiescent, non-proliferative state, and are downregulated in stimulated T-cells undergoing a proliferative burst. In T-cells lacking BTG1 and BTG2, the quiescent state is disrupted, and T-cells readily undergo clonal expansion. This is accompanied by global changes resulting in increased poly(A) tail length, and increased mRNA and protein levels,[4] which is consistent with a general mechanism of recruitment by PABPC1 of the Ccr4-Not deadenylase via BTG1/BTG2 in the non-proliferative state.

In lymphoid malignancies, deadenylation involving Caf1, BTG2 and PABPC1 also appears to be deregulated. Several studies identified frequent missense mutations in BTG1 and BTG2 in non-Hodgkin lymphoma.[5–8] A large proportion of these mutations have been shown to impair the interaction of BTG1 or BTG2 with the Caf1 (CNOT7/CNOT8) deadenylase.[48] In addition, several BTG2 missense mutations have been identified in the region of BTG2 binding to PABPC1 (**Supplementary Figure S5**). Thus, it may be that some of the lymphoma-associated missense mutations in BTG1 or BTG2 also interfere with binding PABPC1. Indeed, PABPC1 has been identified as a possible

driver gene of lymph tumours and recurring mutations in PABPC1 have been identified in several tumour types, including tumours in the upper aerodigestive tract.[9,44] The availability of the BTG2-PABPC1 structural model will provide a framework for the computational evaluation of the impact of cancer-associated variants in BTG2 and PABPC1.

CRediT authorship contribution statement

Aalam Ameerul: Investigation, Methodology, Resources. **Hibah Almasmoum:** Methodology, Resources. **Lorenzo Pavanello:** Methodology, Resources. **Cyril Dominguez:** Formal analysis, Writing – review & editing. **Gerlof Sebastiaan Winkler:** Conceptualization, Supervision, Writing – original draft, Writing – review & editing.

DATA AVAILABILITY

The structural model of BTG2-PABPC1 is available at the PDB-Dev database[49] under accession code PDBDEV_00000099.

Conflict of interest statement

The authors declare no conflicts of interest.

Appendix A. Supplementary data

Supplementary data to this article can be found online at https://doi.org/10.1016/j.jmb.2022.167662.

References

1. Mauxion, F., Chen, C.Y., Seraphin, B., Shyu, A.B., (2009). BTG/TOB factors impact deadenylases. *Trends Biochem. Sci.* **34**, 640–647.
2. Winkler, G.S., (2010). The mammalian anti-proliferative BTG/Tob protein family. *J. Cell. Physiol.* **222**, 66–72.
3. Yuniati, L., Scheijen, B., van der Meer, L.T., van Leeuwen, F.N., (2018). Tumor suppressors BTG1 and BTG2: Beyond growth control. *J. Cell. Physiol.* **234**, 5379–5389.
4. Hwang, S.S., Lim, J., Yu, Z., Kong, P., Sefik, E., Xu, H., et al., (2020). mRNA destabilization by BTG1 and BTG2 maintains T cell quiescence. *Science* **367**, 1255–1260.
5. Lohr, J.G., Stojanov, P., Lawrence, M.S., Auclair, D., Chapuy, B., Sougnez, C., et al., (2012). Discovery and prioritization of somatic mutations in diffuse large B-cell lymphoma (DLBCL) by whole-exome sequencing. *Proc. Natl. Acad. Sci. U. S. A.* **109**, 3879–3884.
6. Morin, R.D., Mendez-Lago, M., Mungall, A.J., Goya, R., Mungall, K.L., Corbett, R.D., et al., (2011). Frequent mutation of histone-modifying genes in non-Hodgkin lymphoma. *Nature* **476**, 298–303.
7. Reddy, A., Zhang, J., Davis, N.S., Moffitt, A.B., Love, C.L., Waldrop, A., et al., (2017). Genetic and functional drivers of diffuse large B cell lymphoma. *Cell* **171** 481-94.e15.
8. Zhang, J., Grubor, V., Love, C.L., Banerjee, A., Richards, K.L., Mieczkowski, P.A., et al., (2013). Genetic heterogeneity of diffuse large B-cell lymphoma. *Proc. Natl. Acad. Sci.* **110**, 1398–1403.
9. Dietlein, F., Weghorn, D., Taylor-Weiner, A., Richters, A., Reardon, B., Liu, D., et al., (2020). Identification of cancer driver genes based on nucleotide context. *Nat. Genet.* **52**, 208–218.
10. Boiko, A.D., Porteous, S., Razorenova, O.V., Krivokrysenko, V.I., Williams, B.R., Gudkov, A.V., (2006). A systematic search for downstream mediators of tumor suppressor function of p53 reveals a major role of BTG2 in suppression of Ras-induced transformation. *Genes Dev.* **20**, 236–252.
11. Kawakubo, H., Brachtel, E., Hayashida, T., Yeo, G., Kish, J., Muzikansky, A., et al., (2006). Loss of B-cell translocation gene-2 in estrogen receptor-positive breast carcinoma is associated with tumor grade and overexpression of cyclin d1 protein. *Cancer Res.* **66**, 7075–7082.

12. Struckmann, K., Schraml, P., Simon, R., Elmenhorst, K., Mirlacher, M., Kononen, J., et al., (2004). Impaired expression of the cell cycle regulator BTG2 is common in clear cell renal cell carcinoma. *Cancer Res.* **64**, 1632–1638.

13. Matsuda, S., Rouault, J., Magaud, J., Berthet, C., (2001). In search of a function for the TIS21/PC3/BTG1/TOB family. *FEBS Lett.* **497**, 67–72.

14. Horiuchi, M., Takeuchi, K., Noda, N., Muroya, N., Suzuki, T., Nakamura, T., et al., (2009). Structural basis for the antiproliferative activity of the Tob-hCaf1 complex. *J. Biol. Chem.* **284**, 13244–13255.

15. Yang, X., Morita, M., Wang, H., Suzuki, T., Yang, W., Luo, Y., et al., (2008). Crystal structures of human BTG2 and mouse TIS21 involved in suppression of CAF1 deadenylase activity. *Nucleic Acids Res.* **36**, 6872–6881.

16. Collart, M.A., Panasenko, O.O., (2012). The Ccr4-not complex. *Gene* **492**, 42–53.

17. Goldstrohm, A.C., Wickens, M., (2008). Multifunctional deadenylase complexes diversify mRNA control. *Nat. Rev. Mol. Cell Biol.* **9**, 337–344.

18. Wahle, E., Winkler, G.S., (2013). RNA decay machines: Deadenylation by the Ccr4-Not and Pan2-Pan3 complexes. *Biochim. Biophys. Acta, Gene Regul. Mech.* **1829**, 561–570.

19. Jonas, S., Izaurralde, E., (2015). Towards a molecular understanding of microRNA-mediated gene silencing. *Nat. Rev. Genet.* **16**, 421–433.

20. Parker, R., Song, H., (2004). The enzymes and control of eukaryotic mRNA turnover. *Nat. Struct. Mol. Biol.* **11**, 121–127.

21. Ezzeddine, N., Chen, C.Y., Shyu, A.B., (2012). Evidence providing new insights into TOB-promoted deadenylation and supporting a link between TOB's deadenylation-enhancing and antiproliferative activities. *Mol. Cell. Biol.* **32**, 1089–1098.

22. Mauxion, F., Faux, C., Seraphin, B., (2008). The BTG2 protein is a general activator of mRNA deadenylation. *EMBO J.* **27**, 1039–1048.

23. Ezzeddine, N., Chang, T.C., Zhu, W., Yamashita, A., Chen, C.Y., Zhong, Z., et al., (2007). Human TOB, an antiproliferative transcription factor, is a poly(A)-binding protein-dependent positive regulator of cytoplasmic mRNA deadenylation. *Mol. Cell. Biol.* **27**, 7791–7801.

24. Stupfler, B., Birck, C., Seraphin, B., Mauxion, F., (2016). BTG2 bridges PABPC1 RNA-binding domains and CAF1 deadenylase to control cell proliferation. *Nat. Commun.* **7**, 10811.

25. Doidge, R., Mittal, S., Aslam, A., Winkler, G.S., (2012). The anti-proliferative activity of BTG/TOB proteins is mediated via the Caf1a (CNOT7) and Caf1b (CNOT8) deadenylase subunits of the Ccr4-not complex. *PLoS ONE* **7**, e51331

26. Amine, H., Ripin, N., Sharma, S., Stoecklin, G., Allain, F.H., Séraphin, B., et al., (2021). A conserved motif in human BTG1 and BTG2 proteins mediates interaction with the poly(A) binding protein PABPC1 to stimulate mRNA deadenylation. *RNA Biol.* **1–16**

27. Funakoshi, Y., Doi, Y., Hosoda, N., Uchida, N., Osawa, M., Shimada, I., et al., (2007). Mechanism of mRNA deadenylation: evidence for a molecular interplay between translation termination factor eRF3 and mRNA deadenylases. *Genes Dev.* **21**, 3135–3148.

28. Dominguez, C., Boelens, R., Bonvin, A.M., (2003). HADDOCK: a protein-protein docking approach based on biochemical or biophysical information. *J. Am. Chem. Soc.* **125**, 1731–1737.

29. van Zundert, G.C.P., Rodrigues, J., Trellet, M., Schmitz, C., Kastritis, P.L., Karaca, E., et al., (2016). The HADDOCK2.2 Web Server: User-Friendly Integrative Modeling of Biomolecular Complexes. *J. Mol. Biol.* **428**, 720–725.

30. de Vries, S.J., Bonvin, A.M., (2011). CPORT: a consensus interface predictor and its performance in prediction-driven docking with HADDOCK. *PLoS ONE* **6**, e17695

31. de Vries, S.J., van Dijk, A.D., Bonvin, A.M., (2006). WHISCY: what information does surface conservation yield? Application to data-driven docking. *Proteins* **63**, 479–489.

32. Neuvirth, H., Raz, R., Schreiber, G., (2004). ProMate: a structure based prediction program to identify the location of protein-protein binding sites. *J. Mol. Biol.* **338**, 181–199.

33. Porollo, A., Meller, J., (2007). Prediction-based fingerprints of protein-protein interactions. *Proteins.* **66**, 630–645.

34. Liang, S., Zhang, C., Liu, S., Zhou, Y., (2006). Protein binding site prediction using an empirical scoring function. *Nucleic Acids Res.* **34**, 3698–3707.

35. Kufareva, I., Budagyan, L., Raush, E., Totrov, M., Abagyan, R., (2007). PIER: protein interface recognition for structural proteomics. *Proteins* **67**, 400–417.

36. Chen, H., Zhou, H.X., (2005). Prediction of interface residues in protein-protein complexes by a consensus neural network method: test against NMR data. *Proteins* **61**, 21–35.

37. Safaee, N., Kozlov, G., Noronha, A.M., Xie, J., Wilds, C.J., Gehring, K., (2012). Interdomain allostery promotes assembly of the poly(A) mRNA complex with PABP and eIF4G. *Mol. Cell* **48**, 375–386.

38. Krissinel, E., Henrick, K., (2007). Inference of macromolecular assemblies from crystalline state. *J. Mol. Biol.* **372**, 774–797.

39. Pavanello, L., Hall, B., Airhihen, B., Winkler, G.S., (2018). The central region of CNOT1 and CNOT9 stimulate deadenylation by the Ccr4-Not nuclease module. *Biochem. J.* **475**, 3437–3450.

40. Maryati, M., Airhihen, B., Winkler, G.S., (2015). The enzyme activities of Caf1 and Ccr4 are both required for deadenylation by the human Ccr4-Not nuclease module. *Biochem. J.* **469**, 169–176.

41. Honorato, R.V., Koukos, P.I., Jimenez-Garcia, B., Tsaregorodtsev, A., Verlato, M., Giachetti, A., et al., (2021). Structural Biology in the Clouds: The WeNMR-EOSC Ecosystem. *Front. Mol. Biosci.* **8**, 729513

42. Schrödinger LLC. The PyMol Molecular Graphics System, version 2.5.0 (open source).

43. Chen, V.B., Arendall 3rd, W.B., Headd, J.J., Keedy, D.A., Immormino, R.M., Kapral, G.J., et al., (2010). MolProbity: all-atom structure validation for macromolecular crystallography. *Acta Crystallogr. D Biol. Crystallogr.* **66**, 12–21.

44. Tate, J.G., Bamford, S., Jubb, H.C., Sondka, Z., Beare, D.M., Bindal, N., et al., (2019). COSMIC: the Catalogue Of Somatic Mutations In Cancer. *Nucleic Acids Res.* **47**, D941–D947.

45. Webster, M.W., Chen, Y.H., Stowell, J.A.W., Alhusaini, N., Sweet, T., Graveley, B.R., et al., (2018). mRNA Deadenylation Is Coupled to Translation Rates by the Differential Activities of Ccr4-Not Nucleases. *Mol. Cell* **70**, (1089–100) e8

46. Yi, H., Park, J., Ha, M., Lim, J., Chang, H., Kim, V.N., (2018). PABP Cooperates with the CCR4-NOT Complex to Promote mRNA Deadenylation and Block Precocious Decay. *Mol. Cell* **70**, (1081–8) e5

47. Zhang, Q., Pavanello, L., Potapov, A., Bartlam, M., Winkler, G.S., (2022). Structure of the human Ccr4-Not nuclease module using X-ray crystallography and electron paramagnetic resonance spectroscopy distance measurements. *Protein Sci.* **31**, 758–764.

48. Almasmoum, H.A., Airhihen, B., Seedhouse, C., Winkler, G.S., (2021). Frequent loss of BTG1 activity and impaired interactions with the Caf1 subunit of the Ccr4-Not deadenylase in non-Hodgkin lymphoma. *Leuk. Lymphoma* **62**, 281–290.

49. Vallat, B., Webb, B., Fayazi, M., Voinea, S., Tangmunarunkit, H., Ganesan, S.J., et al., (2021). New system for archiving integrative structures. *Acta Crystallogr. D Struct. Biol.* **77**, 1486–1496.